A Fault Location Method based on Polynomial Chaos Expansion for Non-uniform Transmission Lines with Uncertainty Parameters

He Shao-Yin, Song Yu, Andréa Cozza, Xie Yan-Zhao, Wang Zhao-Yang

A Fault Location Method based on Polynomial Chaos Expansion for Non-uniform Transmission Lines with Uncertainty Parameters

Shao-yin He, *Senior Member*, *IEEE*, Yu Song, Andrea Cozza, *Senior Member*, *IEEE*, Yan-zhao Xie, *Senior Member*, *IEEE*, and Zhao-yang Wang, *Member*, *IEEE*

***Abstract*—This paper introduces a novel fault location method utilizing polynomial-chaos expansion (PCE) designed specifically for non-uniform transmission lines affected by uncertain parameters. It considers the uncertain parameters arising from height and ground conductivity in transmission lines, examining their impact on conventional fault location methods, such as natural frequency and full-transient analysis approach. These uncertainties lead to considerable location errors, particularly magnified with increasing fault distances. To address this issue, we propose a fault location approach based on PCE and correlation estimation. Simulations cover fault distances ranging from tens to hundreds of kilometers, considering variations in non-uniform line section-lengths, and examining scenarios with single and multiple conductors. Results demonstrate that the proposed method exhibits robustness across different degrees of uncertainty parameters in non-uniform settings, reducing the relative location error to below 1%. In terms of computational efficiency, the PCE method can accelerate calculations by up to 12 times compared to the Monte Carlo method. Furthermore, the PCE method has been validated using fault transient data from an actual 220 kV power line achieving a location error of 2.41%, which demonstrates its practical applicability in real-world power grid scenarios.**

***Index Terms*— Fault location, parameter uncertainty analysis, polynomial chaos expansion, natural frequency analysis, full transient analysis, correlation coefficient, surge compression.**

I. INTRODUCTION

The High Voltage Direct Current (HVDC) transmission system boasts several advantages, including extended transmission distances, reduced line costs, and high transmission capacity [1]. The precise and prompt localization of faults plays a pivotal role in ensuring the safe and stable operation of HVDC systems. The presence of intricate geographical features and challenging terrains can increase the likelihood of faults occurring. Moreover, these factors can complicate the accurate fault localization process for power transmission lines in mountainous area.

In the existing HVDC transmission systems, transmission distances can extend to thousands of kilometers, traversing complex and diverse terrain. Taking the actual HVDC transmission system in China as an example, the Xiangjiaba-Shanghai ±800kV UHVDC transmission project passes through 8 provinces, covering a total length of 1891km. Within this route, precipitous mountains account for 16.26%, general mountains account for 34.41%, hills cover 20.76%, river networks constitute 12.51%, and flat land comprises only 16.06% of the terrain. In the Jinping-Sunan ±800kV UHVDC transmission project, flat land represents merely 9.4% of the total 2059km route [2]. The power transmission line cross through mountainous areas introduces non-negligible uncertainties into the parameters of the transmission line, particularly in terms of line height and ground conductivity. These parameters are closely tied to geographical factors and can exhibit significant variations in such complex geographical regions.

In the event of a fault in the power transmission system, the commonly employed method for fault location is the Traveling Wave Method (TWM), which is widely used in the field of fault location. This method calculates the fault distance based on the time difference [3]. The Frequency-Based Method (FBM) is a specific type of TWM that analyzes resonance frequencies to estimate the length of the faulted line in the frequency domain. The fault distance is determined through the natural frequency, traveling wave velocity, and the phase shift of the reflection coefficient at the transmission line terminal [4]. The accuracy of the location result is closely tied to above three influencing factors.

The Full Transient-Based Method (TBM) avoids the need for waveform feature extraction and relies on the similarity between measured and simulated transients as a localization criterion [5][6]. However, it necessitates a simulation model of the power line that closely approximates reality to ensure a high correlation coefficient.

For traditional TWM and FBM methods, the impact of transmission line parameters on wave velocity is typically

This work was supported in part by the National Natural Science Foundation of China under Grant 52007139, Key R&D Program of Shaanxi Province (2023-YBGY-064). *(Corresponding author: S.-Y. He)*

S.-Y. He, Y Song, and Y.-Z. Xie, are with the State Key Laboratory of Electrical Insulation and Power Equipment, School of Electrical Engineering, Xi'an Jiaotong University, Xi'an 710049, China (email: shaoyin.he@xjtu.edu.cn;songyu645188@stu.xjtu.edu.cn; yzxie@xjtu.edu.cn).

A. Cozza is with the Group of Electrical Engineering - Paris (GeePs), CNRS, CentraleSupelec, Université Paris-Saclay, Sorbonne Universités, 3 & 11 rue Joliot-Curie, Plateau de Moulon 91192 Gif-sur-Yvette CEDEX, France (email: andrea.cozza@ieee.org).

Z.-Y. Wang is with the Communication and Signal Processing Group, Department of Electrical and Electronic Engineering, Imperial College London, SW7 2BX London, U.K. (e-mail: zhaoyang.wang@imperial.ac.uk)

disregarded, and empirical wave velocities are employed for fault location calculations. In the context of HVDC transmission systems, to achieve precise wave velocity, [7] introduced an active pulse injection method. This method utilizes the actions of sub-modules within the Modular Multi-level Converter in High-voltage direct current (MMC-HVDC) system to generate pulses in the transmission line under normal operating conditions for wave velocity determination. Furthermore, the concept of a hybrid circuit breaker has been proposed to produce injecting pulse voltages as well [8]. In contrast, [9] suggested the installation of multiple fault transient measuring devices for wave velocity estimation, although this approach is not recommended for very long lines due to signal attenuation and dispersion of the traveling wave.

To mitigate the influence of traveling wave velocity in the fault location equation, [10] proposed the use of multi-terminal fault signals to eliminate the wave velocity factor in the calculation equation, thereby enhancing accuracy through multi-terminal data. This solution assumes a constant wave velocity, independent of frequency variations, and does not address the frequency-dependent nature of propagation velocity.

Uncertainty quantification in transmission lines has been explored, particularly in the context of field-line coupling. Key research approaches encompass statistical methods based on sampling and polynomial chaos expansion methods [11]. In the realm of sampling-based statistical methods, the widely employed Monte Carlo method demands extensive simulations. The Polynomial Chaos Expansion (PCE) method, originally introduced by N. Wiener [12], has seen substantial development in fields such as vehicle dynamics [13], communication systems [14], and power systems [15], etc. P. Manfredi utilized the PCE technique to systematically investigate the radiation sensitivity of transmission lines and crosstalk between cables [16]-[18]. To the best of the authors' knowledge, there is limited literature addressing uncertainty parameters in fault location for transmission lines, with the exception of [19]. Reference [19] primarily pertains to univariate cases in single conductor lines. It does not account for the stochastic variations in parameters along the transmission line, which arise from the diverse terrain encountered in practical HVDC transmission systems. Additionally, it does not encompass cases involving multiple conductors and multivariable cases as well.

Given the inevitable random variations in height and ground conductivity along the transmission line, the influence of uncertain parameters poses a challenge for existing conventional fault location methods. This paper seeks to mitigate uncertainty-induced location errors introduced by transmission line parameters by integrating the PCE technique with TBM.

The paper is structured as follows: In Sec. II, we illustrate the influence of transmission line parameter uncertainty on traditional fault location methods, using the monopolar HVDC transmission line as an example. Sec. III introduces the theory of combining TBM with PCE. The impact of non-uniform section lengths on the proposed method's location accuracy is discussed in Sec. IV. Sec. V provides a comparison of the performance of various fault location methods, taking into consideration uncertainty parameters in the monopolar HVDC system. Sec. VI delves into the scenario of bipolar HVDC transmission lines. The time consumption and coping optimization strategy is evaluated in Sec. VII. Sec. VIII demonstrates the location ability of the proposed method in an actual power system. Finally, conclusions and discussions are presented in Sec. IX.

II. Assessment Of Transmission Line Parameter Uncertainty To The Fault Location

A. Parameters Analysis for Overhead Lines

In the high voltage power transmission scenario, transmission lines will traverse diverse landscapes involving mountainous regions. In mountainous regions, especially when power lines traverse valleys, the elevation of the line undergoes substantial fluctuations, spanning from tens of meters to hundreds of meters, which often exceed the height of the transmission towers. Concurrently, ground conductivity exhibits a wide range of variation. The long-distance HVDC transmission lines traverse various landforms, resulting in considerable variability in ground conductivity as well [2].

In the presence of random variable ξ_1 in height h and ξ_2 in ground conductivity σ_g, based on transmission line theory [20], the formula of parameters can refer to Appendix A. Due to the uncertainty in these two parameters, the wave velocity will be influenced by uncertainty parameters in transmission line, whose mathematical formula can be written as:

$$v(\xi_1,\xi_2)=\frac{\omega}{\mathrm{Im}\left\{\sqrt{(Z_g^{'}(\xi_1,\xi_2)+Z_w^{'}+j\omega L(\xi_1))(G+j\omega C(\xi_1))}\right\}} \tag{1}$$

Fig.1 shows how the interval of random variation of the velocity varies with the frequency, simulated by Monte Carlo method. The random range of height is [30, 130] m while the ground conductivity is [0.001, 0.1] S/m. The uncertainty range shrinks as the frequency increases. Considering the impact of the height, for 1 kHz, the maximum span of the velocity is 3.182×10^7 m/s, corresponding to an absolute distance bias of 15.91 km, based on the dominant natural frequency, from equation $L=v/2f$. For 100 Hz with the distant fault, the velocity uncertainty 3.5950×10^7 m/s corresponds to a location uncertainty of 180 km; and 2.03×10^7 m/s with an error of 1015 m, at 10 kHz. For the ground conductivity σ_g, the velocity and distance uncertain interval are 3.7470×10^7 m/s, 18.73 km under the natural frequency of 1 kHz. At 10 kHz, the values are 2.031×10^7 m/s, 1015 m respectively. It is evident that these location errors are significant and difficult to be ignored, especially in long-distance power lines.

B. Uncertainty Analysis of Natural Frequency

According to the resonant frequency analysis based on fault transient [4], the line resonance is followed by the equation

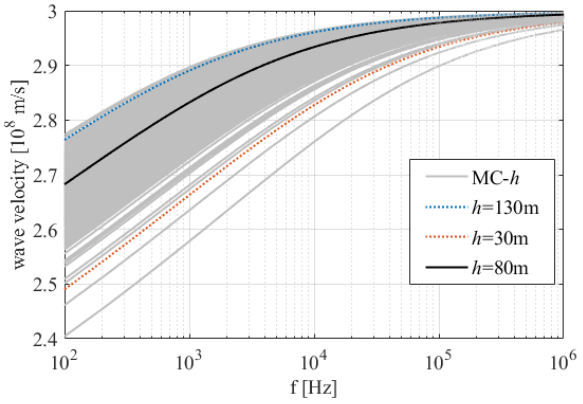

(a)

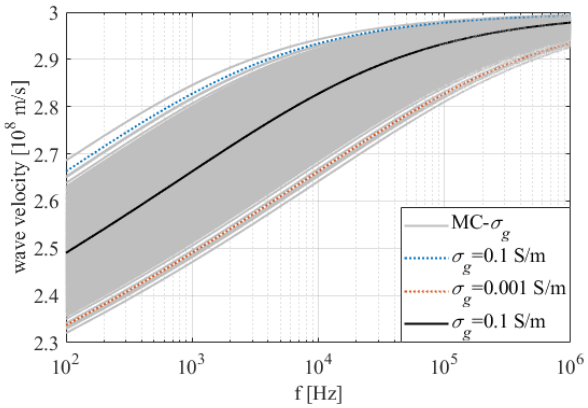

(b)

Fig. 1. Interval of velocity uncertainty changes with frequency, (a) varies according to the height of the line, and (b) varies with ground conductivity.

$$\Gamma_S \Gamma_T e^{-2\alpha L} e^{-2sL/v} = 1 \tag{2}$$

where s is the Laplace variable, the reflection coefficients of the fault and the power-station terminal are represented as Γ_s and Γ_T, respectively. The k-th order resonance frequency ω_k can be computed by solving (3),

$$\omega_k = \frac{v(\omega_k)}{4\pi L}(\theta_S + \theta_T + 2k\pi), k = 0,1,2... \tag{3}$$

where L is the fault distance, θ_S, θ_T are the phase-shift angles of Γ_s and Γ_T. For a low fault impedance short circuit fault, the fault impedance is much lower the line characteristic impedance which means $\Gamma_S \approx -1$, $\theta_S = \pi$. The impact on θ_T by incomplete terminal model has been discussed in [21]. In the following sections, we will assume simplified terminations for the sake of simplicity, although it is worth noting that the proposed method can be extended to more realistic configurations. To emphasize the impact of the transmission process on overhead transmission lines, $\theta_T \approx 0$ is assumed as for a high impedance [22]. The fault distance can be calculated:

$$\hat{L}_k = \frac{\hat{v}(\omega_k)}{4\pi\omega_k}(\pi + 2k\pi), k = 0,1,2... \tag{4}$$

The fault distance $\hat{L}_k$ can be calculated from (4) by the natural angular frequency ω_k, and propagation velocity $\hat{v}(\omega_k)$ which is highly dependent on ω_k. In actual power transmission lines, the presence of uncertain parameters, as indicated in (1),

TABLE I
TRANSMISSION LINE PARAMETERS

Line parameters	Values
Diameter [cm]	42.3
DC resistance [Ω/m]	1.88×10^{-7}
Reference Height [m]	30
Ground conductivity [S/m]	0.01
Fault impendence [Ω]	10
Line length [km]	300

leads to a bias between the assumed $\hat{v}(\omega_k)$ in the calculation process and the true value. The imprecisely estimated wave velocity can result in a nonnegligible fault line distance bias, denoted as $\Delta L_k = \hat{L}_k(\zeta) - L$, where L represents the actual fault distance.

To evaluate the impact of uncertainty parameters in transmission lines on the natural frequency-based fault location method, we created a uniform transmission-line model using MATLAB with the parameters detailed in Table I. Given that the voltage level of the transmission line is 500kV, the tower height is 30m, and the ground conductivity is set as 0.01 S/m. The line radius was determined based on the equivalent radius of the commonly used 500kV split lines. Accounting for variations in topography, the actual height of the transmission line was set within the range of [30, 130] meters, while the conductivity ranged from [0.001, 0.1] S/m. Transmission line parameters would therefore exhibit random variations along the line. When we utilize formulas (3) and (4) to calculate natural frequencies and fault distances, the boundary values of uncertainty were employed to represent extreme mismatches in line parameters.

Based on the parameters in Table I, when uncertainties in the height of the transmission line and ground conductivity are introduced, we present the relative location errors of the natural frequency-based method for distances ranging from 1km to 300km in Fig. 2, based on the natural frequencies computed from (3). Since the height interval is specified as [30, 130]m, with the lower limit representing the reference tower height, only one set of relative error curves is present in Fig. 2(a) when the height is 130m.

In Fig. 2(b), fault natural frequencies are determined for ground conductivities of 0.001 S/m (solid line) and 0.1 S/m (dotted line). Taking into account the parameters uncertainty, the traveling wave velocity in (4) corresponds to the wave velocity associated with frequencies when the reference tower height is 30m and the ground conductivity matches the empirical value of 0.01 S/m.

The results illustrate that within the [1, 300] km range, the line parameters uncertainty leads to a general increase in the relative location errors as the fault distance grows. Additionally, different natural frequency orders are compared in Fig. 2, denoted as n. Utilizing higher-order fault frequencies will reduce the error introduced by the line parameters uncertainty. This indicates that the parameters uncertainty

exerts a more noticeable impact on lower frequencies,

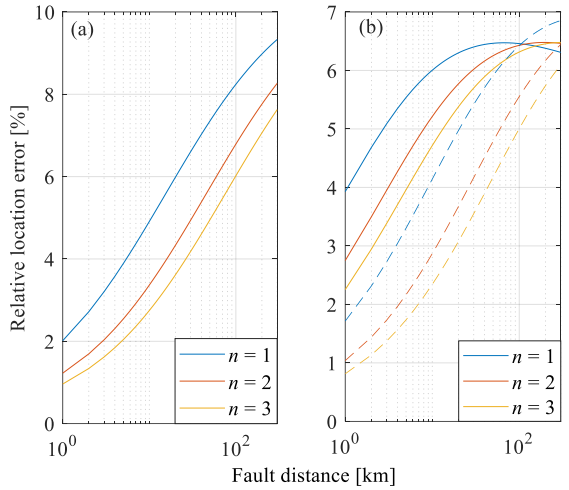

Fig. 2. Relative location error for a different resonance order n involving height and ground conductivity uncertainty, when assuming a nominal velocity: (a) height is 130m and ground conductivity is 0.01 S/m; (b) height is 30m and ground conductivity is 0.001 S/m for solid line while height is 30m and ground conductivity is 0.1 S/m for dotted line.

corresponding to longer fault distances.

C. Location Uncertainty of Full-transient Correlation Estimator Method

Taking the occurrence of a short-circuit fault as an example, the fault transient $v_m(t,L)$ is measured and recorded by the voltage sensor at the terminal with a fault distance of L. During the simulation or precomputation phase in TBM, multiple simulated voltages $\hat{v}_m(t,\hat{L})$ are collected at different guessed lengths $\hat{L}$. In the existing literature, two location criteria choices are commonly found to provide a quantitative metric. The first one involves a posteriori normalization by the maximum value of the projection, which can be explained as a form of global normalization.

$$P_n(L,L)=\frac{P(L,L)}{\max_x\left|P(L,x)\right|} \tag{5}$$

This projection is used in EMTR (Electromagnetic Time Reversal) norm metrics [24]. Additionally, correlation estimator methods are employed as a position-dependent paradigm [5].

$$\rho(L,L)=\frac{P(L,L)}{\sqrt{P(L,L)P(L,L)}} \tag{6}$$

The correlation estimator essentially represents a linear inner product, and it has been demonstrated to exhibit a more robust performance in lossy [24] or multiple branch transmission line networks [25]. In the TBM correlation-based method, fault positions are estimated based on the maximum $\rho(L,\hat{L})$. It is known that the correlation estimator fault location method relies on the impulse response correlation coefficient maximum criterion [5]. The line impulse response h_m can be estimated from the measured transient v_m by applying inverse filtering and surge compression, as detailed in [26].

It is clear that a specific fault distance L will produce a certain ω_k for a given parameter configuration. However, when stochastic transmission line parameters are considered, there is a shift bias between ω_k and $\hat{\omega}_k$, leading to two consequences: the maximum correlation coefficient will be less than one, and the peak value of the correlation coefficient will shift towards the error location.

III. Full Transient Based Fault Location Method Combined With PCE

The conventional approach to address stochastic problems involves conducting a substantial number of deterministic simulations with random parameters, creating a database of random responses. The Monte Carlo (MC) method is a classic example of this approach. However, its primary drawback is the significant computational burden it imposes. On the other hand, the polynomial chaos expansion approach offers the capability to provide statistical information with much higher efficiency compared to MC analysis.

A. Transmission Line Modelling by PCE

The primary concept behind the PCE is to represent a stochastic unknown response in the form of a polynomial expansion to approximate the actual system output response [27]. The PCE technique involves a spectral expansion of a stochastic process $y(\xi)$ using a truncated series of orthogonal polynomials. Following the Askey scheme, PCE approximates $y(\xi)$ mathematically as follows:

$$y(\xi)\approx y(\xi)=\sum_{k=0}^{P}c_k\phi_k(\xi) \tag{7}$$

where P is the order of the expansion, $\phi_k(\xi)$ is the orthogonal polynomial basis, c_k are the unknown coefficients in the expression. We can determine the coefficients through Galerkin projection.

$$c_k=\left\langle y(\xi),\phi_k(\xi)\right\rangle\approx\left\langle\sum_{i=0}^{P}c_i\phi_i(\xi),\phi_k(\xi)\right\rangle \tag{8}$$

The $\phi_k(\xi)$ are orthonormal with respect to the inner product defined as

$$\left\langle\phi_m,\phi_n\right\rangle=\int_{-\infty}^{+\infty}\phi_m(\xi)\phi_n(\xi)w(\xi)d\xi=\delta_{mn} \tag{9}$$

The function $w(\xi)$ serves as the weight function that resembles the Probability Density Function (PDF) of the random variable ξ.

TABLE II
Winner – Askey Polynomial Expansion

Distribution	Polynomial Chaos	Weight function	Range
Normal	Hermite	$e^{-x^2/2}/\sqrt{2\pi}$	(-∞, +∞)
Uniform	Legendre	1/2	[-1, +1]
Gamma	Laguerre	$\frac{x^{\alpha}e^{-x}}{\Gamma(\alpha+1)}$	[0, +∞)
Beta	Jacobi	$\frac{(1-x)^{\alpha}(1+x)\beta}{2^{\alpha+\beta+1}B(\alpha+1,\beta+1)}e^{-x}$	[-1, +1]

The Wiener-Askey scheme offers a guideline for selecting the optimal polynomial basis shown in Table II. Considering a single conductor overhead line above a lossy ground, the height h is treated as a random parameter. As a result of this stochastic variable input, the deterministic transfer function will yield a stochastic output response. We assume that h follows a normal distribution with a range of [30, 130]m,

$$h = \mu_h + \sigma_h \xi \tag{10}$$

Here, μ_h represents the mean value, σ_h denotes the standard deviation of h and ξ is the random variable. Consequently, the telegraph equation for the transmission line, taking into account parameter uncertainty, can be expressed as:

$$\begin{aligned} \frac{d}{dz}V(z,\omega,\xi) &= -Z(\omega,\xi)I(z,\omega,\xi) \\ \frac{d}{dz}I(z,\omega,\xi) &= -Y(\omega,\xi)V(z,\omega,\xi) \end{aligned} \tag{11}$$

where

$$\begin{aligned} Z(\omega,\xi) &= R(\omega,\xi) + j\omega L(\omega,\xi) \\ Y(\omega,\xi) &= G(\omega,\xi) + j\omega C(\omega,\xi) \end{aligned} \tag{12}$$

The per-unit-length parameters Z and Y, as well as the responses V and I, are represented in the PCE format as:

$$\begin{aligned} Z(\omega,\xi) &\approx Z(\omega,\xi) = \sum_{k=0}^{P} Z_k(\omega)\phi_k(\xi) \\ Y(\omega,\xi) &\approx Y(\omega,\xi) = \sum_{k=0}^{P} Y_k(\omega)\phi_k(\xi) \\ V(z,\omega,\xi) &\approx V(z,\omega,\xi) = \sum_{k=0}^{P} V_k(z,\omega)\phi_k(\xi) \\ I(z,\omega,\xi) &\approx \hat{I}(z,\omega,\xi) = \sum_{k=0}^{P} I_k(z,\omega)\phi_k(\xi) \end{aligned} \tag{13}$$

Substitute (13) into (11):

$$\begin{aligned} \frac{d}{dz}\sum_{k=0}^{P} V_k(z,\omega)\phi_k(\xi) &= -\sum_{k=0}^{P}\sum_{j=0}^{P} Z_k(\omega) I_j(z,\omega)\phi_k(\xi)\phi_j(\xi) \\ \frac{d}{dz}\sum_{k=0}^{P} I_k(z,\omega)\phi_k(\xi) &= -\sum_{k=0}^{P}\sum_{j=0}^{P} Y_k(\omega) V_j(z,\omega)\phi_k(\xi)\phi_j(\xi) \end{aligned} \tag{14}$$

Take the inner product of both sides of (14)

$$\begin{aligned} \begin{bmatrix} \vdots \\ \frac{d}{dz}V_i \\ \vdots \end{bmatrix} &= -\begin{bmatrix} \cdots & \sum_{k=0}^{P} Z_k \frac{\langle \phi_k\phi_j, \phi_i \rangle}{\langle \phi_i, \phi_i \rangle} & \cdots \end{bmatrix} \begin{bmatrix} \vdots \\ I_j \\ \vdots \end{bmatrix} \\ \begin{bmatrix} \vdots \\ \frac{d}{dz}I_i \\ \vdots \end{bmatrix} &= -\begin{bmatrix} \cdots & \sum_{k=0}^{P} Y_k \frac{\langle \phi_k\phi_j, \phi_i \rangle}{\langle \phi_i, \phi_i \rangle} & \cdots \end{bmatrix} \begin{bmatrix} \vdots \\ V_j \\ \vdots \end{bmatrix} \end{aligned} \tag{15}$$

where $\alpha_{kji} = \frac{\langle \phi_k\phi_j, \phi_i \rangle}{\langle \phi_i, \phi_i \rangle}$, $\tilde{V} = [V_0, \ldots, V_p]^T$, $\tilde{I} = [I_0, \ldots, I_p]^T$, (15) can be further represented in matrix format.

$$\begin{aligned} \frac{d}{dz}\mathbf{V}(z,\omega) &= -\mathbf{Z}(\omega)\tilde{\mathbf{I}}(z,\omega) \\ \frac{d}{dz}\tilde{\mathbf{I}}(z,\omega) &= -\mathbf{Y}(\omega)\mathbf{V}(z,\omega) \end{aligned} \tag{16}$$

The matrix $\tilde{\mathbf{Z}}$, $\tilde{\mathbf{Y}}$ are $(P+1)\times(P+1)$ dimensional square matrix which is produced by multiplying matrices $\mathbf{Z}$ and α.

$$\begin{aligned} Z_{ij}(\omega) &= \sum_{k=0}^{P} Z_k(\omega)\alpha_{kij} \\ Y_{ij}(\omega) &= \sum_{k=0}^{P} Y_k(\omega)\alpha_{kij} \end{aligned} \tag{17}$$

According to the principles of TBM, the transmission line model should be constructed based on the prior information of the power grid system. If the parameters are deterministic, the transfer function can be computed straightforwardly. However, when we account for uncertainty in the parameters of the model, an analytical approach using the chain parameters matrix is employed to solve equation (17).

B. Proposed Fault Location Algorithm Based on PCE

Due to the uncertainty disparity between real parameters and simulated parameters, an inherent location bias arises in the correlation estimator method. Additionally, the maximum correlation coefficient ρ is less than 1, indicating a mismatch between measurements and simulations. To address this issue, we have introduced a novel full transient-based fault location algorithm, which combines the correlation estimator with PCE. The detailed process is outlined as follows:

1) Collect prior information, including conductor line and tower structure, power grid topology, ground electrical parameters, and other relevant data.
2) Simulate fault transients using the uncertainty proxy model of the transfer function based on the PCE. Create a database of fault transients for different guessed fault locations. Once the proxy model is established, it allows for rapid synthesis of fault responses for all partitioned locations and heights (using random variables as an example). Solving the proxy model provides coefficients for orthogonal polynomials, which can be used to obtain fault responses, as shown in (8), corresponding to all random variables for a specific fault location.
3) Measure and record the actual fault transients. Apply surge compression strategy to the measured and simulated transient signals to estimate the transfer functions $H_m(\omega)$ and $H_s(\omega)$ of the fault-transient spectra $V_m(\omega)$ and $V_s(\omega)$, as detailed in [26].
4) Calculate the correlation coefficient ρ_{HH} between the proxy model and the fault transient transfer functions H_s and H_m.
5) Correlation ρ_{HH} will vary with the stochastic variation (ξ_1, ξ_2, ...ξ_n,$\hat{L}$). Set (ξ_1, ξ_2, ...ξ_n) and estimated position $\hat{L}$ corresponding to the maximum ρ_{HH}. The fault position is then determined by the following condition:

$$x_f = \arg\max \left\| \rho_{HH}(\xi_1, \xi_2, \ldots, \xi_n, L) \right\| \quad (18)$$

When calculating the correlation coefficient in a frequency band containing finite *m* frequency points, each one results in an equation, for a total of *m* equations. However, the independent variables considered are the uncertainty parameters and the fault distance, and the number of independent variables is much smaller than the number of equations, making the solution unique. When the correlation coefficient is equal to 1, it will yield parameters perfectly consistent with the real system. Although the resolution of constraint variables may prevent the occurrence of a correlation coefficient equal to 1, due to the uniqueness of the solution, the values of the independent variables obtained in the solution will approach the unique solution.

PCE is introduced to efficiently model the transmission line, taking into account uncertainty parameters, and obtain the line parameters that closely match the realistic values by considering the maximum correlation coefficient. This optimization ultimately enhances the location reliability. The overall method can be likened to exploring all positions and all random variables. The construction of the surrogate PCE model simplifies the process of acquiring fault responses for all random variables, making it more straightforward and efficient.

IV. Impact Of The Non-uniform Section-length To Location Accuracy

Taking the single conductor line from Table I as an example, the total length of the line is divided into different sections, and the number of divided sections is used to model the non-uniformity of the transmission line. The height of the transmission line in each section is randomly generated within the interval [30, 130] m following a truncated normal distribution, as mentioned in Sec. II. In this section, the transmission line with a total length of 300 km is evenly divided into 30, 300, and 3000 sections, resulting in section lengths of 10 km, 1 km, and 100 m, respectively. A section length of 100 m implies an impedance discontinuity every 100 m. In MC simulation, 100 verification simulations are conducted for each section length. The height used in each simulation is randomly generated within the height interval. A performance comparison between the TBM and the proposed method is presented in Fig. 3.

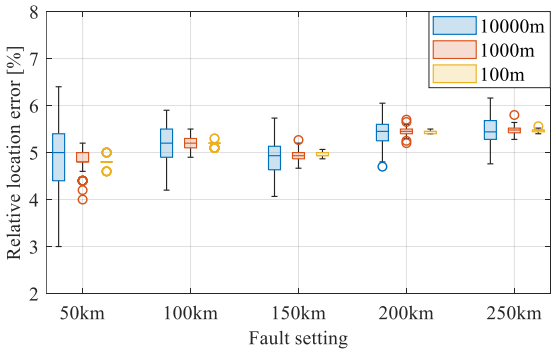

(a)

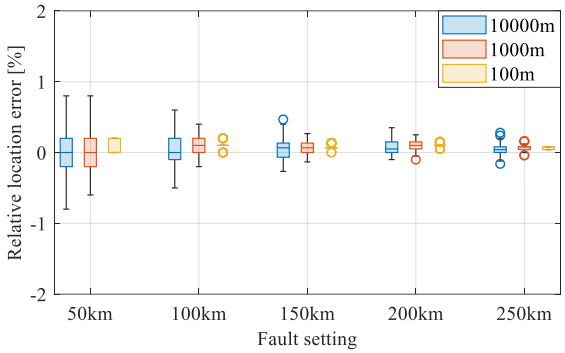

(b)

Fig. 3. Relative location error comparison of TBM and proposed method for different lengths of uniform line sections: (a) TBM method (b) PCE method. The boxes represent the 50% probability margin of relative error, the short horizontal black lines mark the upper and lower limits corresponding to the 99.3% probability margin of relative error, while the circles represent outliers with a probability of 0.7%.

For TBM, the ground conductivity used is 0.01 S/m, and the height is set to the reference tower height of 30 m, with the height uncertainty ignored. At different fault distances and for different degrees of non-uniformity along the line, the location error of TBM is approximately 5%. For TBM, the maximum range of the 99.3% probability margin is [3%, 6.4%], the 50% confidence interval is [4.4%, 5.4%], and the maximum median is 5.45%. For the proposed PCE method, the relative errors are significantly reduced and fall within the ranges of [-0.8%, 0.8%], [-0.2%, 0.2%], and 0% for the section lengths of 10km, 1km and 100m. Additionally, the error range becomes narrower as the section length decreases. This is because non-uniform uncertainty changes tend to have a weaker impact on the location result for shorter line lengths. In other words, longer line sections are associated with higher relative error rates.

In the Fault Generated Phase (FGP), the height varies from 30 m to 130 m, while the estimated height remains fixed at 30 m during the Simulation Phase (SP). Consequently, the velocity of the traveling wave is lower in the FGP than in the SP, leading to positive location errors at different fault distances, shown as Fig. 3(a). When the height *h* follows a normal distribution, the estimated fault distance may be shorter or longer than the actual position, resulting in location errors that could be negative or positive in Fig. 3(b). The proposed PCE method significantly improves the relative location error, reducing it from the range of [3%, 6.4%] to [-0.8%, 0.8%] with a 99.3% confidence interval.

V. Single-Conductor Overhead Line

In the previous section, the robustness of the proposed method in relation to the section length of a non-uniform transmission line was demonstrated through MC simulations. In this section, using a single conductor transmission line as an example, we consider uncertainties in both the height and ground conductivity when the transmission line spans a long distance. We provide numerical examples to quantify distance uncertainty when univariate and multivariate uncertainty

parameters exist in the line. These examples serve to demonstrate the effectiveness of the proposed method. Furthermore, we also compare the location performance between traditional fault location methods and the proposed method.

A. Height Uncertainty Analysis

It is assumed that the height of the transmission line follows a normal distribution [27], which can be represented as $h=80+\frac{50}{3}\xi$. According to the formulas (8)-(14) in Sec. III, Hermite orthogonal polynomials are used to expand Z and Y, which include uncertain parameters up to the second order.

Once the Z and Y matrices of the expanded circuit are determined using the PCE, the fault response of the expanded circuit is computed within the frequency range of 1 Hz to 10 kHz using the chain parameter calculation formula. This process allows for the creation of a proxy model for the fault response shown as:

$$V_s(t)=\sum_{k=0}^{P}V_k(t)\phi_k(\xi) \tag{19}$$

Fig. 4 displays the normalized proxy model of the fault response when a 10 Ω short-circuit-to-ground fault occurs at 100 km. In Fig. 4, the red curve represents the fault response of the transmission line when the height is 30 m, and the grey area represents the fault response of the transmission line when the height varies between 30 and 130 m. When the transmission line traverses areas with significant terrain fluctuations, such as mountains, the actual height of the transmission line may not align with the true height of the tower. As shown in Fig. 4, the fault response of the transmission line exhibits considerable variations in such scenarios.

In Sec. IV, we demonstrated the robustness of the proposed method with respect to the degree of inhomogeneity in the transmission line's height. Therefore, in this section, to save computational time, the 300 km transmission line is divided into 30 sections, and the height of each section is randomly generated between 30m and 130 m according to a normal distribution.

To illustrate the location process of the proposed method, Fig. 5 presents the location results for a short-circuit fault at 100 km. With the height following a normal distribution, the change in ξ within the range of [-3, 3] corresponds to the variation in height within [30, 130] m. For each ξ value, the corresponding height $h=80+\frac{50}{3}\xi$ can be determined in the proxy model of formula (19). The reference fault response at different fault locations under ξ can be used in formula (6) to compute the correlation coefficient curve at height $h(\xi)$, and the fault location corresponding to the maximum correlation coefficient is the result for $h(\xi)$.

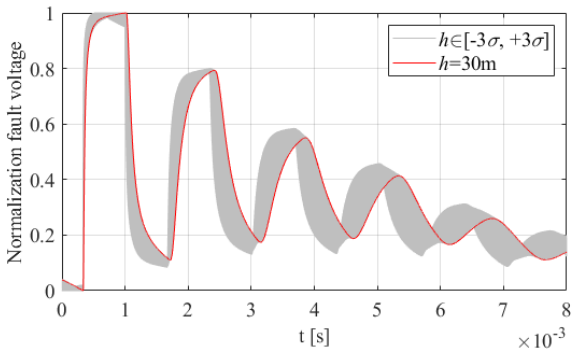

Fig. 4. Normalization fault voltage at 100km.

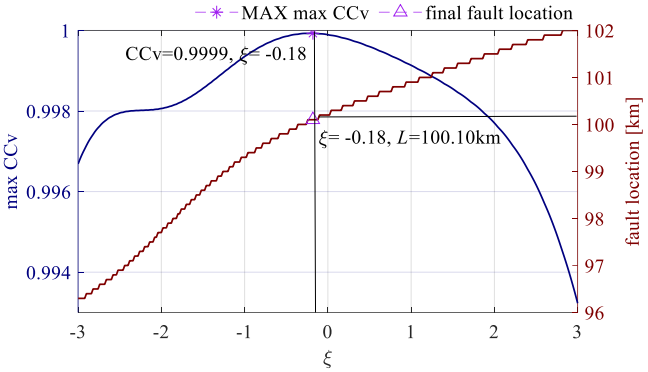

Fig. 5. The location process of the proposed method at 100km. The asterisk denotes the coordinate (CCv=0.9999, ξ=-0.18), while the upward-pointing triangle represents (ξ=-0.18, L=100.10 km).

Therefore, as shown in Fig.5, the maximum correlation coefficient value (CCv) corresponding to every ξ and the corresponding location result can be obtained. The correlation coefficient represents the similarity between the reference fault signal and the actual fault signal. The only difference between the reference transmission line and the actual transmission line is the height and the fault distance. Actually, the fault transient varies with line height h and fault distance L. While calculating the correlation coefficient in a certain frequency band, although the correlation coefficient is only a single value, during the calculation process, every frequency point in the frequency band is equivalent to an equation to be solved, which is equivalent to solving an overdetermined equation system about h and L. At this time, h and L have the unique solution.

TABLE III
CONSIDERING HEIGHT UNCERTAINTY IN SINGLE-CONDUCTOR OVERHEAD LINE

Fault length [km]	TWM $\Delta\epsilon/\left\|\frac{\Delta\epsilon}{L}\right\|$	FBM $\Delta\epsilon/\left\|\frac{\Delta\epsilon}{L}\right\|$	TBM $\Delta\epsilon/\left\|\frac{\Delta\epsilon}{L}\right\|$	PCE $\Delta\epsilon/\left\|\frac{\Delta\epsilon}{L}\right\|$
50	-3.40/6.80%	-2.91/5.82%	-2.22/4.44%	0.40/0.80%
100	-6.80/6.80%	-5.61/5.61%	-5.12/5.12%	0.10/0.10%
150	-13.53/9.02%	-9.40/6.27%	-7.72/5.15%	0.10/0.07%
200	-16.93/8.47%	-12.41/6.21%	-10.82/5.41%	0.30/0.15%
250	-20.33/8.13%	-16.04/6.42%	-13.52/5.41%	0.10/0.04%

$\Delta\epsilon$ is the absolute location error, $\left|\frac{\Delta\epsilon}{L}\right|$ is the relative location error.

Hence, when $h(\xi)$ approaches the height of the actual transmission line, the maximum correlation coefficient obtained becomes larger. As shown in Fig. 5, the maximum correlation coefficient reaches its maximum value along the ξ variation curve. At this point, it is considered that the $h(\xi)$ corresponding to the maximum value is closest to the height of the actual transmission line, and the fault location corresponding to the maximum value is the final location result.

Table III presents a comparison of the location results using different fault location methods under non-uniform height conditions along the transmission line. The single-ended traveling wave method and the natural frequency-based method (FBM) both utilize line parameter settings with a reference tower height of 30m and a ground conductivity of 0.01 S/m. The fault location is determined by TWM after extracting the time delay when the traveling wave arrives at the measuring point twice in a row. However, due to the influence of height uncertainty on wave velocity, as shown in Table III, TWM exhibits a significant location error, with a relative location error of up to 9.02% at 150km.

In the natural frequency-based method, due to the influence of the uncertain parameters, the relative location error at the set fault location is around 6%. For TBM, the height of the tower is also used as the line parameter when the reference signal is generated. Due to the mismatch of the transmission line height, the fault resonance peak shifts over the entire frequency band, resulting in a relative location error of about 5% at the set fault location.

In the proposed method, the 300km line is divided into 10 km steps, and the calculation frequency band is set to [1Hz, 10kHz] with a frequency step of 1Hz. After solving the proxy model along the line, the maximum value of the correlation coefficient in the proxy model is determined. The results demonstrate that the proposed method, when compared to traditional fault location methods, can reduce the location error to less than 1%. The relative location error is less than 0.1% at distances of 100km, 150km, and 250km. This indicates that the proposed method is applicable for fault location in scenarios involving nonuniform height along the transmission line.

TABLE IV
CONSIDERING GROUND CONDUCTIVITY UNCERTAINTY IN SINGLE CONDUCTOR OVERHEAD LINE

Fault length L [km]	TWM $\Delta\epsilon/\left\lvert\frac{\Delta\epsilon}{L}\right\rvert$	FBM $\Delta\epsilon/\left\lvert\frac{\Delta\epsilon}{L}\right\rvert$	TBM $\Delta\epsilon/\left\lvert\frac{\Delta\epsilon}{L}\right\rvert$	PCE $\Delta\epsilon/\left\lvert\frac{\Delta\epsilon}{L}\right\rvert$
50	-0.08/0.02%	2.18/4.36%	1.68/3.36%	0.10/0.20%
100	-0.15/0.15%	3.94/3.94%	3.62/3.62%	0.20/0.20%
150	-3.55/-2.37%	5.63/3.75%	4.40/2.93%	-0.10/0.08%
200	6.37/3.19%	7.53/3.77%	7.04/3.52%	-0.20/0.10%
250	9.62/3.85%	9.76/3.90%	8.90/3.56%	0.20/0.08%

B. Ground Conductivity Uncertainty Analysis

Typically, when creating a simulation model for a transmission line, a ground conductivity value of 0.01 S/m is assumed. However, in this section, we aim to assess whether the proposed fault location method can effectively handle transmission lines with varying ground conductivity along different length. Being consistent with Sec. V-A, we divided a 300km transmission line into 30 sections to replicate an actual scenario where ground conductivity is not uniform. The ground conductivity within each segment is generated using a lognormal distribution within the range of [0.001, 0.01] S/m, as detailed in reference [28],[29].

The mean value of this distribution is approximately 0.003 S/m, which significantly deviates from the typical value of 0.01 S/m. This deviation is introduced to replicate scenarios where ground conductivity varies substantially along the transmission line. The comparison of location results for different methods is presented in Table IV. While TWM performs relatively well at fault distances of 50km and 100km, its accuracy diminishes for other fault distances, resulting in a relative location error of approximately 3%. For FBM, relative location errors of 2% to 5% are observed at various fault distances. The TBM also experiences a relative location error of about 3% due to ground conductivity discrepancies. In contrast, the proposed method effectively mitigates the issue of a ground conductivity mismatch, reducing the relative location error to less than 1%. Furthermore, at the specified fault distance, absolute location errors do not exceed 200m for fault distances of 250 km.

C. Height and Ground Conductivity Uncertainties Analysis

In Sec. V-A and B, we provide comparisons of various fault location methods in scenarios where single uncertain parameters existed in the transmission line. However, in real-world transmission lines, variations in both height and ground conductivity can occur simultaneously due to the diverse landforms they traverse. In this section, we introduce a fault location method that considers multiple uncertain parameters and provide simulation cases to illustrate its performance.

The multivariate fault location method presented in this section is fundamentally similar to the univariate approach, as it also relies on the largest correlation coefficient as the key indicator for fault location. The primary distinction between the multivariate and single-variable applications is found in equation (8). When applying PCE to model line parameters that encompass multiple sources of uncertainty, the orthogonal polynomial basis employed becomes a tensor product of the individual univariate orthogonal polynomial bases. Specifically, for the height and ground conductivity parameters, which utilize Hermite orthogonal polynomials as their basis, the multivariate expansion employs tensor products of these Hermite orthogonal polynomial bases.

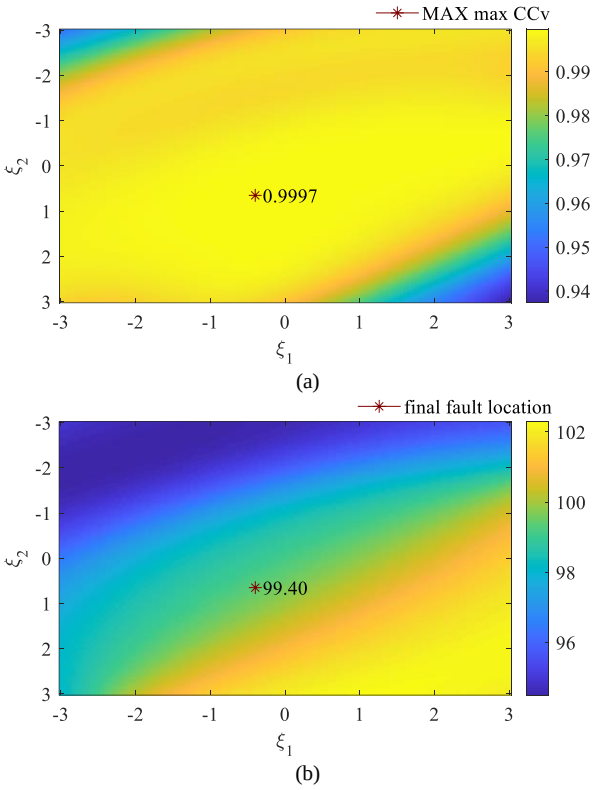

Fig.6. The location process of the proposed method at 100km while multivariate uncertainty parameters existing. (a) The max correlation coefficient curve corresponding to ξ_1 and ξ_2, (b) The guessed position based on the maximum correlation coefficient corresponding to different random variables ξ_1 and ξ_2.

$$\begin{cases} \phi_0(\boldsymbol{\xi}) = \phi_0(\xi_1)\phi_0(\xi_2) = 1 \\ \phi_1(\boldsymbol{\xi}) = \phi_1(\xi_1)\phi_0(\xi_2) = \xi_1 \\ \phi_2(\boldsymbol{\xi}) = \phi_0(\xi_1)\phi_1(\xi_2) = \xi_2 \\ \phi_3(\boldsymbol{\xi}) = \phi_2(\xi_1)\phi_0(\xi_2) = (\xi_1^2 - 1)/\sqrt{2} \\ \phi_4(\boldsymbol{\xi}) = \phi_1(\xi_1)\phi_1(\xi_2) = \xi_1\xi_2 \\ \phi_5(\boldsymbol{\xi}) = \phi_0(\xi_1)\phi_2(\xi_2) = (\xi_2^2 - 1)/\sqrt{2} \end{cases} \tag{20}$$

When the multivariate expansion is carried out up to the second order, the **ZY** matrix will transform into a 6×6 matrix. By solving the fault response of this expanded circuit, a fault response proxy model is established, taking into account uncertainties in both the transmission line height and ground conductivity. Subsequently, the fault location can be executed following the same computational process as in the case of univariate uncertainty parameters.

Fig. 6 presents the fault location results for a 10 Ω short-circuit fault occurring at a distance of 100 km when there are uncertainties in both the height and ground conductivity. The simulation settings used to generate the actual fault signal align with those in Sec. V-A and B. The 300 km transmission line is divided into 30 sections, and the height and conductivity of each section utilize the same random numbers as in the previous sections. In the figure, ξ_1 represents height, and ξ_2 represents ground conductivity. When the correlation coefficient reaches its maximum value, the location result is 99.40 km, with a relative error of only 0.6%.

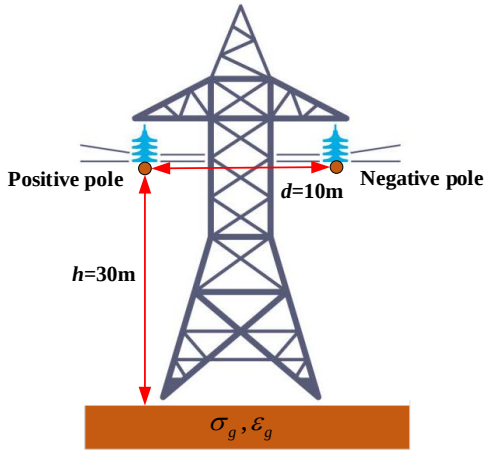

Fig.7. Bipolar HVDC transmission line structure

TABLE V
CONSIDERING HEIGHT AND GROUND CONDUCTIVITY UNCERTAINTIES IN SINGLE CONDUCTOR OVERHEAD LINE

Fault length L [km]	TWM $\Delta\epsilon/\lvert\frac{\Delta\epsilon}{L}\rvert$	FBM $\Delta\epsilon/\lvert\frac{\Delta\epsilon}{L}\rvert$	TBM $\Delta\epsilon/\lvert\frac{\Delta\epsilon}{L}\rvert$	PCE $\Delta\epsilon/\lvert\frac{\Delta\epsilon}{L}\rvert$
50	-3.40/6.80%	-1.62/3.24%	-1.30/2.60%	0.10/0.20%
100	-6.80/6.80%	-4.69/4.69%	-4.00/4.00%	-0.60/0.60%
150	-10.20/6.80%	-7.91/5.23%	-6.00/4.00%	0.30/0.20%
200	-13.60/6.80%	-10.26/5.13%	-9.10/4.55%	0.70/0.35%
250	-17.00/6.80%	-14.37/5.75%	-12.30/4.92%	-0.50/0.20%

Without loss of generality, Table V provides the location results at different fault distances. In comparison with the location errors of the traditional method in Table III, the relative location errors of the traditional method in this section are generally reduced. This reduction occurs because the randomly generated height and ground conductivity have opposite effects on transmission line propagation concerning the transmission line parameters. The randomly generated height tends to increase the **ZY** parameters of the line, whereas the randomly generated conductivity has the opposite effect. Therefore, under the influence of both factors, the relative location error of the traditional fault location algorithm is smaller than that in Table III, ranging between 2% and 8%.

However, the proposed method can reduce the location error caused by multivariate uncertainty to less than 1%. At the set fault location, the method proposed in this paper exhibits a maximum relative location error of 0.6%.

VI. MULTICONDUCTOR OVERHEAD LINE

This section sets out to verify that the phenomena in the case of the multiconductor overhead line. Take the bipolar HVDC transmission lines for example, there is coupling between the positive and negative poles. The similarity transformation is adopted to decouple the phasor signal into modal signals as explained in [20].

$$\begin{cases} \begin{bmatrix} u_0 \\ u_1 \end{bmatrix} = \frac{1}{\sqrt{2}} \begin{bmatrix} 1 & 1 \\ 1 & -1 \end{bmatrix} \begin{bmatrix} u_{\mathrm{p}} \\ u_{\mathrm{n}} \end{bmatrix} \\ \begin{bmatrix} i_0 \\ i_1 \end{bmatrix} = \frac{1}{\sqrt{2}} \begin{bmatrix} 1 & 1 \\ 1 & -1 \end{bmatrix} \begin{bmatrix} i_{\mathrm{p}} \\ i_{\mathrm{n}} \end{bmatrix} \end{cases} \tag{21}$$

where the subscripts p and n denote the positive and negative poles, the subscripts 1 and 0 denote the 1-mode and 0-mode components based on the positive pole, respectively. To investigate the impact of uncertainty parameters on the fault location of bipolar HVDC transmission lines, both univariate and multivariate uncertainty parameters are considered in the context of fault location for these transmission lines.

A. Height Uncertainty Analysis

A bipolar HVDC transmission line is modeled in MATLAB. Fig. 7 illustrates a cross-section of the transmission line under investigation, which is representative of the 500 kV power towers commonly used in China.

Using a positive pole-to-ground fault as an example, Table VI presents the location results obtained from different mode components following the pole-mode transformation. It is noticeable that the impact on the 1-mode component is reduced and the relative location error is substantially smaller, with some fault distances exhibiting errors of less than 1%, which meets the actual requirements of the project. However, pole-mode transformation cannot entirely eliminate the influence of uncertain line parameters on the 1-mode components, resulting in noticeable location errors, particularly evident at a distance of 200km, for instance. Nevertheless, due to the cumulative effect of uncertain parameters, the relative location error for the 0-mode component increases significantly in comparison to the 1-mode component. When using the proposed method, the location error can be entirely eliminated when employing the 1-mode component at the specified fault distances. Additionally, the relative location error can also be reduced to below 1% even when using the 0-mode component.

B. Ground Conductivity Uncertainty Analysis

Continuing from the extreme ground conductivity scenario described in Sec.V-B, a bipolar transmission line with nonuniform ground conductivity along its length is established, focusing on pole-to-ground fault. After applying pole-mode transformation to the fault response, the location results from various methods are presented in Table VII. The results indicate that the proposed method can reduce the relative error to less than 0.2%, regardless of whether the 0-mode or 1-mode component is used. This demonstrates that the proposed method exhibits robustness against parameter uncertainty in the context of bipolar transmission lines with nonuniform ground conductivity.

TABLE VI
CONSIDERING HEIGHT UNCERTAINTY IN DOUBLE CONDUCTOR OVERHEAD LINE

Fault length L [km]		TWM $\Delta\epsilon/\left\lvert\frac{\Delta\epsilon}{L}\right\rvert$	FBM $\Delta\epsilon/\left\lvert\frac{\Delta\epsilon}{L}\right\rvert$	TBM $\Delta\epsilon/\left\lvert\frac{\Delta\epsilon}{L}\right\rvert$	PCE $\Delta\epsilon/\left\lvert\frac{\Delta\epsilon}{L}\right\rvert$
50	0	-7.49/14.98%	-1.39/2.78%	-2.30/4.60%	0.30/0.60%
	1	2.41/4.82%	-0.80/1.76%	-0.50/1.00%	0/0%
100	0	-12.70/12.70%	-3.58/3.58%	-4.40/4.40%	-0.10/0.10%
	1	1.07/1.07%	-2.77/2.77%	-0.80/0.08%	0/0%
150	0	-19.94/13.29%	-4.73/3.15%	-3.80/2.53%	-0.30/0.20%
	1	-0.26/0.17%	-4.42/2.94%	7.20/4.80%	0/0%
200	0	-20.92/10.46%	-5.24/2.57%	-14.20/7.10%	0/0%
	1	-1.60/0.80%	-4.58/2.29%	-3.90/1.95%	-0.10/0.05%
250	0	-11.91/4.76%	-7.19/2.88%	-19.90/7.96%	0/0%
	1	-2.93/1.17%	-1.87/0.75%	1.00/0.40%	0/0%

TABLE VII
CONSIDERING GROUND CONDUCTIVITY UNCERTAINTY IN DOUBLE CONDUCTOR OVERHEAD LINE

Fault length L [km]		TWM $\Delta\epsilon/\left\lvert\frac{\Delta\epsilon}{L}\right\rvert$	FBM $\Delta\epsilon/\left\lvert\frac{\Delta\epsilon}{L}\right\rvert$	TBM $\Delta\epsilon/\left\lvert\frac{\Delta\epsilon}{L}\right\rvert$	PCE $\Delta\epsilon/\left\lvert\frac{\Delta\epsilon}{L}\right\rvert$
50	0	-4.49/8.98%	-0.58/1.16%	1.90/3.80%	0.10/0.20%
	1	4.28/8.56%	0.15/0.30%	0.90/1.80%	0/0%
100	0	-2.65/2.65%	-2.39/2.39%	3.60/3.60%	-0.20/0.20%
	1	-0.05/0.05%	0.17/0.17%	1.60/1.60%	-0.10/0.10%
150	0	-11.25/7.50%	-2.87/1.91%	4.00/2.67%	-0.60/0.40%
	1	-0.26/0.17%	1.01/0.67%	-0.50/0.33%	0/0%
200	0	26.94/13.47%	-2.21/1.11%	7.50/3.75%	-0.20/0.10%
	1	-0.10/0.05%	0.97/0.49%	-0.80/0.40%	-0.20/0.10%
250	0	-1.25/0.50%	-4.89/1.96%	10.90/4.36%	-0.10/0.04%
	1	0.06/0.02%	-3.38/1.35%	3.30/1.32%	0/0%

TABLE VIII
CONSIDERING HEIGHT AND GROUND CONDUCTIVITY UNCERTAINTIES IN DOUBLE CONDUCTOR OVERHEAD LINE

Fault length L [km]		TWM $\Delta\epsilon/\left\lvert\frac{\Delta\epsilon}{L}\right\rvert$	FBM $\Delta\epsilon/\left\lvert\frac{\Delta\epsilon}{L}\right\rvert$	TBM $\Delta\epsilon/\left\lvert\frac{\Delta\epsilon}{L}\right\rvert$	PCE $\Delta\epsilon/\left\lvert\frac{\Delta\epsilon}{L}\right\rvert$
50	0	-7.01/14.02%	-4.50/9.00%	-1.30/2.60%	0.30/0.60%
	1	-0.21/0.42%	3.73/7.46%	-0.10/0.20%	0/0%
100	0	-11.50/11.50%	-2.36/2.36%	-2.70/2.70%	0/0%
	1	-0.05/0.05%	-0.83/0.83%	-0.10/0.10%	0/0%
150	0	-18.52/12.35%	-3.49/2.33%	-3.40/2.27%	-0.10/0.07%
	1	-0.26/0.17%	1.27/0.85%	-0.80/0.53%	0/0%
200	0	-26.16/13.08%	-7.34/3.67%	-10.10/5.05%	-0.20/0.10%
	1	-0.47/0.24%	2.37/1.19%	0.10/0.05%	0/0%
250	0	-10.42/4.17%	-7.19/2.88%	-15.70/6.28%	-0.60/0.24%
	1	-0.31/0.12%	-4.56/1.82%	-0.80/0.32%	0/0%

C. Height and Ground Conductivity Uncertainties Analysis

In the context of multiple uncertainty parameters in bipolar DC transmission lines, following the height and ground conductivity settings described in Sec. V-C, and after performing pole-mode transformation on the fault signal. As shown in Table VIII, the relative location error for the traveling wave method and TBM is no more than 1% when using the 1-mode component for location. However, significant location errors occur when using the 0-mode component. In contrast, the proposed method exhibits

outstanding location performance for both 0-mode and 1-mode components, with the largest relative error being 0.6%, observed when using the 0-mode component at 50km. When the 1-mode component is employed, the location error can be completely eliminated at the set fault distances.

VII. Time Consumption of Method

As illustrated in Sec. III.B, the PCE method comprises two parts: pre-simulation procedure and online calculation procedure. In the pre-simulation phase, specific to a transmission line, the necessary computations are conducted in advance to generate a simulation database encompassing parameter uncertainties. Subsequently, when a fault transient is detected in the real power system, the only remaining task is to calculate the correlation between the measured fault signal and the simulation database. Given the consideration of uncertainty parameters, numerous simulations and calculations are likely conducted in pre-simulation for each scenario.

Therefore, the simulation time is approached from two perspectives. The calculation platform employed is an i5-12400K CPU with the memory size of 16GB. Firstly, using a single-conductor over lossy ground as an example, we compare simulation times for a specific simulated fault location. This comparison is between employing Polynomial Chaos Expansion (PCE) to establish a simulated fault response proxy model and using Monte Carlo (MC) sampling for simulated fault responses under various random variables. Table III below illustrates the comparison, where 300 samplings are conducted for both MC and proxy models. The results indicate that utilizing PCE can significantly reduce time consumption, especially when establishing a fault signal proxy model along the line.

TABLE IX
Time-Consuming Comparison of PCE and MC in Pre-simulation Phase

Method	PCE	MC
Time [s]	1.01	12.57

Secondly, to achieve real-time or near-real-time fault localization, a heuristic acceleration algorithm is utilized in the calculation process of correlation coefficients between the actual fault signal and simulation databases [30]. Using a single-conductor transmission line over lossy ground as an example, the calculation times for determining the maximum correlation coefficient at 100 km are provided using exhaustive calculation and the heuristic algorithm. The step of the random variable ξ is set at 0.05 within the range of [-3, 3]. During online calculation, the adoption of the heuristic algorithm significantly reduces the localization time, facilitating real-time or near-real-time fault localization scenario.

TABLE X
Time-Consuming Comparison of Exhaustive Calculation and Heuristic Algorithm in Online Calculation Phase

Uncertainty parameter	Exhaustive calculation	Heuristic algorithm
h	27.13 s	0.78 s
h and σ_g	2876.69s	2.54s

VIII. Experimental validation

The location performance of the proposed method was also tested in a real power line with uncertain height and soil conductivity for a real phase-to-ground fault transient recorded in a 220 kV AC power line in a mountain region, in Yunnan Province, China. The structure diagram of the cross section of the tower is shown in Fig.8. The power line length is 192 km which contains 389 towers in all, the phase-to-ground fault occurred in the phase C of No. 77 tower, with fault distance of 37.29 km.

The measured fault transient currents in the time and frequency domains are depicted in Fig. 9. The sampling rate of the recording equipment was 1 MHz, and the overall recording duration 1.25 ms. In Fig. 8, the time difference between the arrivals of the first two traveling signals is 0.23 ms. In TWM, the traveling wave propagation velocity is estimated using an approximate value of $1/\sqrt{LC}$, which may introduce location errors due to signal velocity bias arising from frequency variation [31]. In this study, the velocity corresponding to the main natural resonance frequency of 4.77 kHz is utilized for calculations, with a value set at 2.83×10^8 m/s. Consequently, the fault position is estimated as 32.55 km using TWM.

When employing FBM, to enhance the resolution and accuracy of the location results, high-order natural frequencies are extracted for fault location [21],[25]. In Fig. 9(b), five orders of resonant frequency are extracted, specifically 21.94 kHz, 26.06 kHz, 30.50 kHz, 34.99 kHz, and 38.98 kHz. By incorporating the traveling wave velocity corresponding to each frequency, the final average location result is determined to be 34.27 km.

Considering the effect of the uncertainty in the transmission line height on the propagation velocity and attenuation, the line model is based by the method of PCE according to the real configuration of the tower in Fig.8. The line height is set to obey a normal distribution in the range of [15m, 45m]. In Fig.10, the CCv and fault position varies with ξ, with the fault position finally estimated for a maximum CCv=0.9153 which is found at a 36.39 km distance. According to the electrical company, the real fault distance was found at 37.29 km.

A comparison of the location results of different methods is given in Table XI. TWM and FBM have a non-negligible absolute location error of 4.74 km and 3.02 km which both exceed 5%. By contrast, PCE limits the error to 0.9 km with a relative location error of 2.41%.

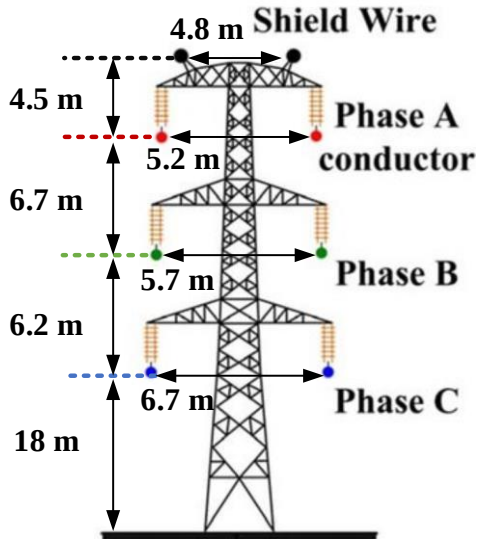

Fig. 8. The cross section of the 220 kV transmission line tower in the actual project.

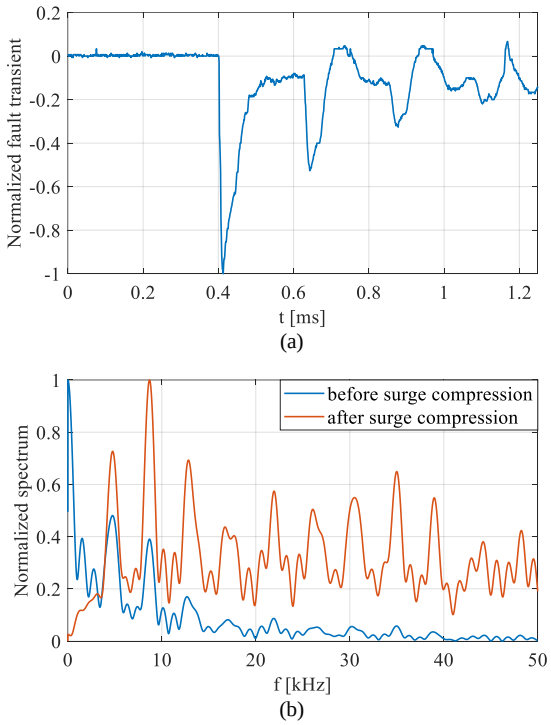

Fig. 9. The measured transient current in time and frequency domain.

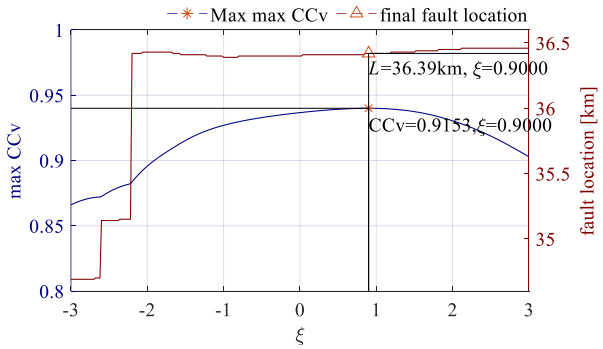

Fig. 10. The CCv and fault position estimation results by actual fault data.

TABLE XI
LOCATION RESULTS OF DIFFERENT METHOD UNDER THE ACTUAL FAULT DATA

Method	Absolute error [km]	Relative error [%]
TWM	4.74	12.72
FBM	3.02	9.13
PCE	0.9	2.41

IX. DISCUSSIONS AND CONCLUSION

This paper focuses on achieving precise fault location for short-circuit ground faults in power-transmission lines affected, by uncertainties related to the conductor height and the ground conductivity. These uncertainties are prevalent in existing power transmission systems due to varying terrains. Using a single-conductor transmission line above a lossy ground as an example, the impact of parameter uncertainties on parameters of the transmission line is examined. The research also presents relative location errors resulting from parameter uncertainties in the natural frequency-based method. For single-conductor transmission lines, it is observed that parameter uncertainties can lead to relative location errors of up to approximately 9%.

A novel location method robust against such uncertainties is introduced, based on a polynomial-chaos expansion approach, while exploiting the ability of full-transient based methods to measure the similarity between measured fault transients and reference propagation models. Results indicate that the proposed method exhibits a very high robustness when dealing with non-uniform degrees of uncertainty parameters along the line, with location errors systematically within 1 %.

The paper provides several comparisons of the location performance between existing fault location methods and the proposed method in both monopolar and bipolar HVDC transmission lines. In monopolar HVDC transmission lines, uncertainties related to line height and ground conductivity can result in substantial relative location errors in traditional fault location methods. In bipolar HVDC transmission lines, due to pole-mode transformation, the influence of uncertainty parameters on the 1-mode component is weakened. However, the 0-mode component is more susceptible to uncertainty parameters, making traditional fault location methods ineffective in this case. In contrast, the proposed method, when used for fault location, consistently delivers accurate results, whether employing 1-mode or 0-mode components, with relative location errors remaining below 1%.

It is also shown that the computation-intensive simulation phase required in full-transient methods is accelerated by PCE, with a reduction in the computation duration by up to 12 times compared to a Monte Carlo method. Additionally, for achieving real-time fault localization scenarios, a heuristic optimization algorithm can complete a simulation case in 2.54 seconds, whereas exhaustive calculation takes 2876.69 seconds.

Finally, the practical performance of PCE is validated using recorded fault current data in actual 220 kV power grid. PCE effectively reduces the relative location error to 2.41%, compared to relative errors of 12.72% and 9.13% for TWM and FBM, respectively.

Future work will extend these results to more additional phenomena of multi-modal propagation and more fault type.

APPENDIX

A. The per-unit-length parameters

The per-unit-length parameters of the single overhead conductor can be expressed as:

$$L^{'}(\xi_1)=\frac{\mu_0}{2\pi}\ln\frac{2h(\xi_1)}{r_w},\ C^{'}(\xi_1)=\frac{2\pi\varepsilon_0}{\ln\frac{2h(\xi_1)}{r_w}},$$

$$Z_g^{'}(\xi_1,\xi_2)=\frac{j\omega\mu_0}{2\pi}\ln\frac{1+\gamma_g(\xi_2)h(\xi_1)}{\gamma_g(\xi_2)h(\xi_1)},\ Z_w^{'}=\frac{1}{\pi r_w^2\sigma_w},\quad(1)$$

$$G^{'}=\frac{\sigma_{air}}{\varepsilon_0},\ Y_g^{'}(\xi_2)=\frac{\gamma_g{}^2}{Z_g^{'}(\xi_2)}$$

Where $L^{'}$ is inductance in series, $C^{'}$ is the capacitance in parallel, $Z_g^{'}$ is the ground impedance in series, $Z_w^{'}$ is the conductor impedance in series, $G^{'}$ is the admittance and $Y_g^{'}$ is the ground admittance in parallel. γ_g is the propagation constant in the ground with $\gamma_g(\xi_2)=\sqrt{j\omega\mu_0(\sigma_g(\xi_2)+j\omega\varepsilon_0\varepsilon_g)}$. The μ_0, ε_0, σ_{air} are electrical parameters of the air; σ_g, ε_g are electrical parameters of the ground; r_w, h are radius and height of the conductor.

B. Fault transient calculation by chain parameter

In this paper, all simulations are carried out in MATLAB and the fault response is calculated by chain parameter.

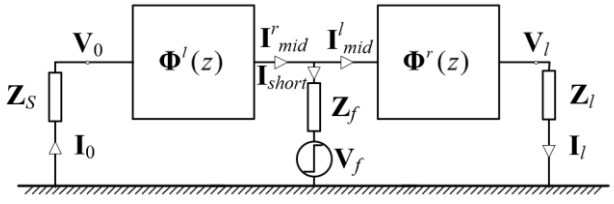

Fig. 11. Chain parameter equation diagram.

In figure 10, $\mathbf{V}_0$ and $\mathbf{I}_0$ are the fault voltage and current at line head, and $\mathbf{V}_l$ and $\mathbf{I}_l$ are the fault voltage and current at line end. At the fault node, transmission line is divided into left and right parts. $\mathbf{I}_{short}$ is the fault branch current, $\mathbf{I}_{mid}^{r}$ and $\mathbf{I}_{mid}^{l}$ is the current flowing before and after the fault node, $\mathbf{\Phi}^{r}$ and $\mathbf{\Phi}^{l}$ are the chain parameters of the two sections, specifically:

$$\mathbf{\Phi}(z)=\begin{bmatrix}\mathbf{\Phi}_{11}(z) & \mathbf{\Phi}_{12}(z)\\ \mathbf{\Phi}_{21}(z) & \mathbf{\Phi}_{22}(z)\end{bmatrix}\quad(2)$$

In which

$$\begin{aligned}\mathbf{\Phi}_{11}(z)&=\frac{1}{2}\mathbf{Y}^{-1}\mathbf{T}_I(\mathbf{e}^{\gamma z}+\mathbf{e}^{-\gamma z})\mathbf{T}_I{}^{-1}\mathbf{Y}\\ \mathbf{\Phi}_{12}(z)&=-\frac{1}{2}\mathbf{Y}^{-1}\mathbf{T}_I\gamma(\mathbf{e}^{\gamma z}-\mathbf{e}^{-\gamma z})\mathbf{T}_I{}^{-1}\\ \mathbf{\Phi}_{21}(z)&=-\frac{1}{2}\mathbf{T}_I(\mathbf{e}^{\gamma z}-\mathbf{e}^{-\gamma z})\gamma^{-1}\mathbf{T}_I{}^{-1}\mathbf{Y}\\ \mathbf{\Phi}_{22}(z)&=\frac{1}{2}\mathbf{T}_I(\mathbf{e}^{\gamma z}+\mathbf{e}^{-\gamma z})\mathbf{T}_I{}^{-1}\end{aligned}\quad(3)$$

Defining the positive direction of current from the beginning of the line to the end of the line, and the boundary conditions from the beginning and end of the line are:

$$\begin{aligned}\mathbf{I}_0&=-\mathbf{Z}_s^{-1}\mathbf{V}_0\\ \mathbf{I}_l&=\mathbf{Z}_l^{-1}\mathbf{V}_l\end{aligned}\quad(4)$$

Therefore, the calculation formula of the chain parameters from line head to the fault node is:

$$\begin{bmatrix}\mathbf{V}_{mid}\\ \mathbf{I}_{mid}^{r}\end{bmatrix}=\begin{bmatrix}\mathbf{\Phi}_{11}^{r}(z) & \mathbf{\Phi}_{12}^{r}(z)\\ \mathbf{\Phi}_{21}^{r}(z) & \mathbf{\Phi}_{22}^{r}(z)\end{bmatrix}\begin{bmatrix}\mathbf{V}_0\\ -\mathbf{Z}_s^{-1}\mathbf{V}_0\end{bmatrix}\quad(5)$$

The calculation formula of the chain parameters from the fault node to line end is:

$$\begin{bmatrix}\mathbf{V}_l\\ \mathbf{Z}_l^{-1}\mathbf{V}_l\end{bmatrix}=\begin{bmatrix}\mathbf{\Phi}_{11}^{l}(z) & \mathbf{\Phi}_{12}^{l}(z)\\ \mathbf{\Phi}_{21}^{l}(z) & \mathbf{\Phi}_{22}^{l}(z)\end{bmatrix}\begin{bmatrix}\mathbf{V}_{mid}\\ \mathbf{I}_{mid}^{l}\end{bmatrix}\quad(6)$$

Thus, the current around the fault node can be expressed by the voltage $\mathbf{V}_0$ as

$$\begin{aligned}\mathbf{I}_{mid}^{l}&=\mathbf{\Phi}_{21}^{l}(z)\mathbf{V}_0-\mathbf{\Phi}_{22}^{l}(z)\mathbf{Z}_s^{-1}\mathbf{V}_0\\ \mathbf{I}_{mid}^{r}&=[\mathbf{\Phi}_{12}^{r}(z)-\mathbf{Z}_l\mathbf{\Phi}_{22}^{r}(z)]^{-1}[\mathbf{Z}_l\mathbf{\Phi}_{21}^{r}(z)-\mathbf{\Phi}_{11}^{r}(z)]\\ &\quad[\mathbf{\Phi}_{11}^{l}(z)-\mathbf{\Phi}_{12}^{l}(z)\mathbf{Z}_s^{-1}]\mathbf{V}_0\end{aligned}\quad(7)$$

At the fault node, the boundary conditions between the line current and the fault node current are:

$$\mathbf{I}_{mid}^{l}=\mathbf{I}_{short}+\mathbf{I}_{mid}^{r}\quad(8)$$

In which

$$\mathbf{I}_{short}=\mathbf{Y}_f(\mathbf{V}_{mid}-\mathbf{V}_f)\quad(9)$$

Above all, the expression of the fault voltage at line head in the frequency domain is derived as:

$$\begin{aligned}\mathbf{V}_0=\{&[\mathbf{Y}_f+[\mathbf{\Phi}_{12}^{r}(z)-\mathbf{Z}_l\mathbf{\Phi}_{22}^{r}(z)]^{-1}[\mathbf{Z}_l\mathbf{\Phi}_{21}^{r}(z)-\mathbf{\Phi}_{11}^{r}(z)]]\\ &[\mathbf{\Phi}_{11}^{l}(z)-\mathbf{\Phi}_{12}^{l}(z)\mathbf{Z}_s^{-1}]-[\mathbf{\Phi}_{21}^{l}(z)-\mathbf{\Phi}_{22}^{l}(z)\mathbf{Z}_s^{-1}]\}^{-1}\\ &\mathbf{Y}_f\mathbf{V}_f\end{aligned}\quad(10)$$

REFERENCE

[1] R. Bertho, V. A. Lacerda, R. M. Monaro, J. C. M. Vieira and D. V. Coury, "Selective Nonunit Protection Technique for Multiterminal VSC-HVDC Grids," *IEEE Transactions on Power Delivery*, vol. 33, no. 5, pp. 2106-2114, Oct. 2018, doi: 10.1109/TPWRD.2017.2756831.

[2] Z. Y. Liu, "Ultra-high voltage AC&DC grid," China Electric Power Press, 2015.

[3] V. P. Dardengo, J. F. Fardin, and M. C. de Almeida, "Single-terminal fault location in HVDC lines with accurate wave velocity estimation," *Electric Power Systems Research*, vol. 94, April. 2021.

[4] Z. Y. He, K. Liao, X. P. Li, S. Lin, J. W. Yang and R. K. Mai, "Natural Frequency-Based Line Fault Location in HVDC Lines," *IEEE Transactions on Power Delivery*, vol. 29, no. 2, pp. 851-859, April. 2014, doi: 10.1109/TPWRD.2013.2269769.

[5] S. He, A. Cozza and Y. Z. Xie, "Electromagnetic Time Reversal as a Correlation Estimator: Improved Metrics and Design Criteria for Fault Location in Power Grids," *IEEE Transactions on Electromagnetic*

Compatibility, vol. 62, no. 2, pp. 598-611, April. 2020, doi: 10.1109/TEMC.2019.2904841.

[6] M. Farshad and J. Sadeh, "A Novel Fault-Location Method for HVDC Transmission Lines Based on Similarity Measure of Voltage Signals," *IEEE Transactions on Power Delivery*, vol. 28, no. 4, pp. 2483-2490, Oct. 2013, doi: 10.1109/TPWRD.2013.2272436.

[7] T Bi, S Wang, and K Jia. "Single pole‐to‐ground fault location method for MMC‐HVDC system using active pulse," *IET Generation, Transmission & Distribution*, vol 12, no.2, pp. 271-278, Jan. 2018.

[8] G. Song, T. Wang and K. S. T. Hussain, "DC Line Fault Identification Based on Pulse Injection From Hybrid HVDC Breaker," *IEEE Transactions on Power Delivery*, vol. 34, no. 1, pp. 271-280, Feb. 2019, doi: 10.1109/TPWRD.2018.2865226.

[9] J. Ding, L. Li, Y. Zheng, C. Zhao, H. Chen, and X. Wang. "Distributed travelling‐wave‐based fault location without time synchronization and wave velocity error," *IET Generation, Transmission & Distribution*, vol. 11, no. 8, pp. 2085-2093, June. 2017.

[10] V. P. Dardengo, P. A. H. Cavalcante and M. C. de Almeida, "An evaluation of wave speed impacts on fault location methods for HVDC lines," 2018 IEEE PES Transmission & Distribution Conference and Exhibition - Latin America (T&D-LA), Lima, Peru, 2018, pp. 1-5, doi: 10.1109/TDC-LA.2018.8511734.

[11] J. P. Yang, "Study on Field-Line Coupling Effect of Random Nonuniform and Terminally Nonlinear Load Transmission Lines," Ji Lin University, 2019.

[12] N. Wiener. "The Homogeneous Chaos." *American Journal of Mathematics*, vol. 60, no. 4, pp. 897–936, Oct. 1938.

[13] F. Ling. "Uncertainty Analysis of Vehicle Suspension Systems Based on Polynomial Chaos Methods," Huazhong University of Science & Technology, 2013.

[14] H Q Zhao, and J S Zhang. "Adaptive nonlinear channel equalization based on combination neural network for chaos-based communication systems," *Acta Phys. Sin.*, vol. 57, no. 7, pp. 3996-4006, July. 2008.

[15] L. Li, Y. Qiu, H. Wu, Y. Song and L. Xiao, "Uncertainty analysis of power system time-domain simulation based on generalized polynomial chaos method," 2017 IEEE Power & Energy Society General Meeting, Chicago, IL, USA, 2017, pp. 1-5, doi: 10.1109/PESGM.2017.8274321.

[16] I. S. Stievano, P. Manfredi and F. G. Canavero, "Parameters Variability Effects on Multiconductor Interconnects via Hermite Polynomial Chaos," *IEEE Transactions on Components, Packaging and Manufacturing Technology*, vol. 1, no. 8, pp. 1234-1239, Aug. 2011, doi: 10.1109/TCPMT.2011.2152403.

[17] I. S. Stievano, P. Manfredi and F. G. Canavero, "Stochastic Analysis of Multiconductor Cables and Interconnects," *IEEE Transactions on Electromagnetic Compatibility*, vol. 53, no. 2, pp. 501-507, May. 2011, doi: 10.1109/TEMC.2011.2119488.

[18] P. Manfredi and F. G. Canavero, "Polynomial Chaos for Random Field Coupling to Transmission Lines," *IEEE Transactions on Electromagnetic Compatibility*, vol. 54, no. 3, pp. 677-680, June. 2012, doi: 10.1109/TEMC.2012.2193586.

[19] A. Nadeem, Y. Xie, S. He, N. Dong, P. Caccavella and M. Saleem, "On the Accuracy of Correlation Estimator Based Fault Location Methods in Transmission Lines via Polynomial Chaos and Regression Analysis," *IEEE Transactions on Electromagnetic Compatibility*, vol. 65, no. 1, pp. 235-248, Feb. 2023, doi: 10.1109/TEMC.2022.3217949.

[20] C. R. Paul, "Analysis of multiconductor transmission lines," John Wiley & Sons, 2007.

[21] S. Y. He, A. Cozza and Y. Z. Xie, "Fault-Location Accuracy of Natural Frequencies Using Incomplete HVDC Station Models," *IEEE Transactions on Power Delivery*, vol. 38, no. 5, pp. 3677-3687, Oct. 2023, doi: 10.1109/TPWRD.2023.3282873.

[22] Z. Wang, Z. Chen and M. Paolone, "A Data-Driven Fault Location Algorithm Based on the Electromagnetic Time Reversal in Mismatched Media," *IEEE Transactions on Power Delivery*, vol. 37, no. 5, pp. 3709-3721, Oct. 2022, doi: 10.1109/TPWRD.2021.3135429.

[23] S. Y. He *et al*., "Norm Criteria in the Electromagnetic Time Reversal Technique for Fault Location in Transmission Lines," *IEEE Transactions on Electromagnetic Compatibility*, vol. 60, no. 5, pp. 1240-1248, Oct. 2018, doi: 10.1109/TEMC.2018.2806892.

[24] A. Cozza, S. Y. He, and Y. Z. Xie, "Impact of propagation losses on fault location accuracy in full transient-based methods," *IEEE Transactions on Power Delivery*, vol. 36, no. 1, pp. 383–396, 2021, doi: 10.1109/TPWRD.2020.2983323.

[25] S. Y. He, A. Cozza and Y. Z. Xie, "On the Spatial Resolution of Fault-Location Techniques Based on Full-Fault Transients," *IEEE Transactions on Power Delivery*, vol. 35, no. 3, pp. 1527-1540, June 2020, doi: 10.1109/TPWRD.2019.2949914.

[26] A. Cozza, S. Y. He and Y. Z. Xie, "Surge Compression for Improved Fault Location Accuracy in Full Transient-Based Methods," *IEEE Sensors Journal*, vol. 21, no. 2, pp. 995-1008, Jan. 2021, doi: 10.1109/JSEN.2020.2989202.

[27] P. Manfredi, "High-speed interconnect models with stochastic parameter variability," Piemonte: Politecnico di Torino, 2013.

[28] G. N. Scott. "Distribution of soil conductivity and its relation to underground corrosion," *American Water Works Association*, vol. 52, no. 3, pp. 378–392, March. 1960.

[29] Nassereddine M, Rizk J, and Nasserddine G, "Soil resistivity structure and its implication on the pole grid resistance for transmission lines," *International Journal of Electrical and Computer Engineering*, vol. 7, no. 1, pp 41-45, Jan 2013.

[30] Song Y, He S, Xie Y, et al, "A Particle Swarm Optimization Fault Location Method Considering Terminal Reflection Phase Shift," 2023 2nd International Conference on Power Systems and Electrical Technology (PSET), pp: 30-35, 2023.

[31] F. V. Lopes, K. M. Silva, F. B. Costa, W. L. A. Neves and D. Fernandes, "Real-Time Traveling-Wave-Based Fault Location Using Two-Terminal Unsynchronized Data," *IEEE Transactions on Power Delivery*, vol. 30, no. 3, pp. 1067-1076, June 2015, doi: 10.1109/TPWRD.2014.2380774.